Scientific Review Engineering and Environmental Sciences (2025), 34 (3), 305-323

Sci. Rev. Eng. Env. Sci. (2025), 34 (3)

https://srees.sggw.edu.pl

ISSN 1732-9353 (suspended)

eISSN 2543-7496

DOI 10.22630/srees.10277

Received: 24.01.2025 Accepted: 06.08.2025

Kiagus Muhammad AMINUDDIN¹⊠ D



Anis SAGGAFF¹



Mahmood Md TAHIR²



Muhammad FIRDAUS³

- ¹ Sriwijaya University, Civil Engineering Department, Faculty of Engineering, Indonesia
- ² University Teknologi Malaysia, School of Civil Engineering, Construction Research Centre (CRC), Institute for Smart Infrastructure and Innovative Construction (ISIIC), Malaysia

Investigation of failure modes and load-deflection of cold-formed steel connections using sub-assemblage frame tests

Keywords: cold-formed steel, sub-assemblage frame test, failure mode, load-deflection, experimental study

Introduction

Cold-formed steel (CFS) is shaped at ambient temperature through bending and rolling, unlike hot-rolled steel (HRS), which is formed at high temperatures. This process enables more precise shaping and sizing, making CFS ideal for construction applications where accuracy and consistency are essential (Dubina et al., 2012; Yu et al., 2019).



³ Universitas PGRI Palembang, Faculty of Engineering, Civil Engineering Department, Indonesia

The benefits of cold-formed steel (CFS) in construction include its versatility, durability, and sustainability. CFS structures are lightweight yet remarkably strong, providing greater design flexibility and enabling the creation of complex architectural forms. Moreover, CFS is highly resistant to corrosion and requires minimal maintenance, making it a durable and eco-friendly building material. Its recyclability further contributes to sustainability, reducing waste and lowering the overall carbon footprint of construction projects (Johnston et al., 2018; Harini et al., 2020). Overall, the advantages of using cold-formed steel in construction are numerous, making it a popular choice among builders and architects.

However, there are some disadvantages; one major drawback is its higher initial cost compared to other building materials, such as wood or concrete. Additionally, cold-formed steel is more susceptible to buckling due to its thinness. Based on EN 1993-1-1 (European Committee for Standardization [CEN], 2005), CFS is categorized as a Class 4 section, due to a high width-to-thickness ratio.

A connection is part of a structure that is critical in ensuring stability and structural integrity. Proper connections can also help distribute loads evenly, prevent structural failure, and improve the overall performance of the construction project. Research on CFS connections has focused on apex and eaves (Pouladi et al., 2019; Chen et al., 2021; Wang et al., 2021; El-Hadary et al., 2022), trusses (Dar et al., 2020; Fitrah & Nofriyandi, 2020; Song et al., 2020; Bondok et al., 2021), and beam-column structures (Ye et al., 2019; Aminuddin et al., 2020; Firdaus et al., 2020a; Firdaus et al., 2020b; Seok et al., 2022). This recent study is limited to the beam-column connection.

Using finite element analysis, Seok et al. (2022) studied altering the through-plates to improve their usefulness in field applications. The numerical simulation results demonstrated that the proposed connection has an equivalent structural performance to the original design. For practicality, attaching a flange plate perpendicular to the diagonal edge is preferable to prevent buckling of the through-plate.

Research conducted by Ye et al. (2019) focused on an in-depth examination of the improvement of seismic behavior in beam-column bolted connections. Their research aimed to identify enhanced design solutions for CFS frames in connection areas susceptible to earthquakes through friction-slip mechanisms. Research demonstrates that the bolted friction-slip mechanism could significantly improve (by up to 200%) the flexibility, ability to dissipate energy, and damping coefficient of the connections, particularly for Class 3 and Class 4 CFS elements. The findings are used to identify optimal design configurations for enhancing the seismic responsiveness of the beam-column connections during intense

earthquakes. While Class 3 and Class 4 cross-sections do not meet the American Institute of Steel Construction specifications for intermediate and special moment frames, the proposed connection mechanism has demonstrated effectiveness in regions with high seismic activity.

This paper presents an experimental study using a sub-assemblage frame test method to evaluate rectangular and haunched gusset plates. A top-seat angle was added to enhance connection resistance. This application used M12 bolts with a grade of 8.8, suitable for light steel profiles, as fasteners.

Material and methods

The flowchart of the current study, as shown in Figure 1, begins with preparation, where materials and equipment are organized. Next, assembling the specimens involves constructing the cold-formed steel beam-column connections according to the sub-assemblage frame method. Measurement instruments, such as load cells and displacement transducers, are then set up to monitor specimen behavior. The study then examines failure modes to identify structural failure. Finally, load-deflection results are analyzed to assess the connection's performance under a monotonic load.

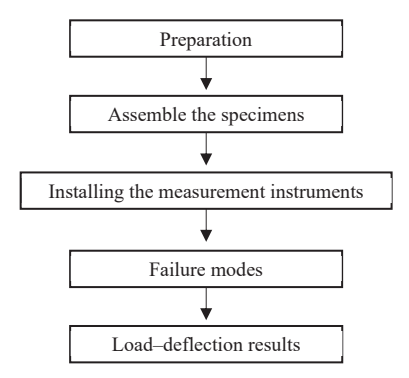


FIGURE 1. Flowchart of the current study

Source: own work.

The arrangement of CFS is back-to-back with double-lipped channel sections. The column section utilized C300, while C200 and C250 were used for the beam section. Each member was designed with grade 450 N·mm⁻², as specified in EN 1993-1-3 (CEN, 2006). The dimensions of the CFS sections are shown in Table 1 and Figure 2.

TABLE 1. Cross-section of cold-formed steel

Cross-section	Depth (d)	Thickness (t)	Flange width (b)	Lip (l)			
Closs-section	mm						
C20024	200	2.4	75	16			
C25024	250	2.4	75	20			
C30024	300	2.4	100	25			

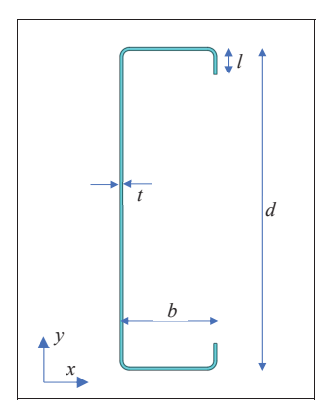
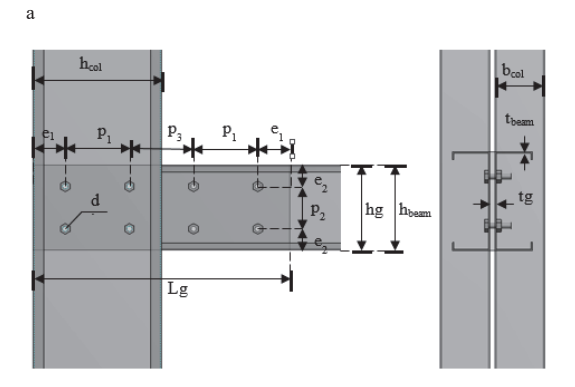


FIGURE 2. Cold-formed steel element

Source: own work.

Three distinct types of connections were employed: a rectangular gusset plate, a rectangular gusset plate with a flange cleat, and a haunched gusset plate. The gusset plate and flange cleat were fabricated from hot-rolled steel to connect the beam and column (Fig. 3, Table 2). Table 2 indicates that the abbreviation SAR denotes a sub-assemblage frame test for a rectangular gusset plate; SARFC signifies a sub-assemblage frame test with a rectangular gusset plate and flange cleat; and SAH represents a sub-assemblage frame test for a haunched gusset plate. Presented here are a few essential terms, as follows: $t_{\rm g}$ denotes the thickness of the gusset plate, $h_{\rm g}$ indicates the height of the gusset plate, $e_{\rm l}$ represents the horizontal distance of the bolt, $e_{\rm l}$ symbolizes the vertical distance of the bolt, $p_{\rm l}$ refers to the horizontal spacing of the bolt, $p_{\rm l}$ relates to the vertical spacing of the bolt, and $p_{\rm l}$ depicts the horizontal spacing of the bolt on both the column and beam.



h_{col}

P₁

P₂

P₂

D_{beam}

D_{beam}

D_{col}

D

b

С

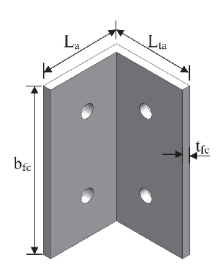
hg₁ Odh OG- Lg

FIGURE 3. Configuration of beam-column connections: (a) rectangular gusset plate, (b) rectangular gusset plate with a top-seat angle, (c) haunched gusset plate

Source: own work.

TABLE 2. Specimen configuration details

Specimen	Beam	Column	Flange cleat	Connection details [mm]							
1			8	t_{g}	h_{g}	$L_{\rm g}$	e_1	e_2	p_1	p_2	p_3
SAR-200	C20024	C30024	_	10	200	600	75	50	150	100	150
SAR-250	C25024	C30024	_	10	250	600	75	50	150	150	150
SARFC-200	C20024	C30024	$L~65\times65\times160$	10	200	600	75	50	150	100	150
SARFC-250	C25024	C30024	$L65\times65\times160$	10	250	600	75	50	150	150	150
SAH-200	C20024	C30024	_	10	400	600	75	50	150	100	150
SAH-250	C25024	C30024	_	10	550	600	75	50	150	150	150



The dimensions of the flange cleat are shown in Figure 4 and Table 3. $t_{\rm fc}$ stands for the thickness of the flange cleat, and $r_{\rm fc}$ for the corner radius of the flange cleat. $l_{\rm a}$ indicates the length of the leg, $l_{\rm ta}$ represents the length of the top leg, $e_{\rm 1a}$ refers to the horizontal edge spacing of the bolt, $e_{\rm 2a}$ represents the vertical edge spacing, and $b_{\rm fc}$ shows the width of the flange cleat.

FIGURE 4. Flange cleat dimensions

Source: own work.

TABLE 3. Flange cleat connection details

Specimens	Beam	Column	Connection details [mm]							
			$t_{ m fc}$	$r_{ m fc}$	$L_{\rm a}$	L_{ta}	e_{1a}	e_{2a}	p_2	$b_{ m fc}$
SARFC-200	C20024	C30024	6	5	65	65	32.5	32.5	85	160
SARFC-250	C25024		6	5	65	65	32.5	32.5	85	160

Source: own work.

The span in this study was 4,000 mm, a typical construction dimension. Six samples were tested, each containing two proposed specimens. The arrangement of the sub-assemblage frame test specimen within the Magnus frame is shown, along with the precise locations of the load cell and spreader beam (Fig. 5). The Magnus frames were organized according to the specimen's structural configuration. A pump-equipped hydraulic jack applied the load, with a load cell positioned at the center, and the spreader beam placed at two points separated

by a two-meter distance. The distance of the spreader beam is based on a quarter of the length of the beam span to ensure the bending condition of the beam. The load was incrementally applied to a value between 0.2 and 0.5 kN using a hydraulic jack.

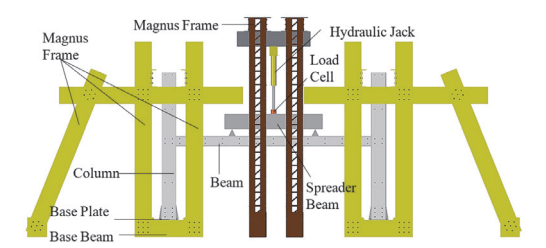


FIGURE 5. Schematic diagram of the sub-assemblage frame test and boundary conditions Source: own work.

The sub-assemblage tests feature full-scale construction with a connecting beam spanning two columns positioned 4,000 mm apart. The gusset-plate connection is placed 1,500 mm from the column center, with the column height measuring 3,000 mm. The beam dimensions are categorized into two sizes: C200 and C250. The columns, on the other hand, have a standard section dimension of C300 with a grade of 450 $\rm N\cdot mm^{-2}$, according to EN 1993-1-3 (CEN, 2006) specifications.

Eleven LVDT units are employed, with LVDTs 1–3 positioned at the beam's midpoint, precisely where the highest moment occurs. LVDTs 8–11 are mounted horizontally on both web columns, while LVDTs 4–7 are arranged to capture accurate vertical deformation (Fig. 6).

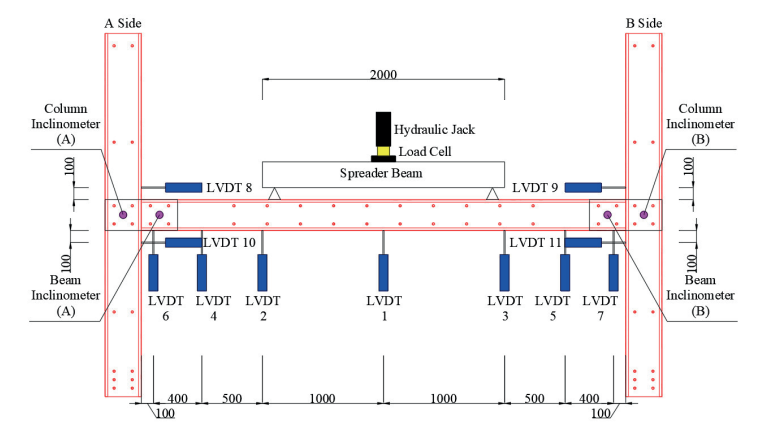


FIGURE 6. Instrument position on the specimen

The test concluded upon observing either a visible failure mode or a sudden and significant displacement increase. The examination identified the failure mechanisms, including buckling at the column flange and substantial rotation of the connection due to bearing failure at the bolt hole. Additionally, thorough visual monitoring was carried out during all examinations, encompassing visual and physical inspections and video documentation for animation. Photographs were taken of each significant item, location, and incident.

Results and discussion

A monotonic load distributed at two points was applied to the beam (Fig. 7). The SAR-200 failure mechanism appears to occur in the compression zone of both the column flange and the bottom beam flange (Fig. 8). This is due to the bottom of the beam flange pushing toward the face of the column flange.



FIGURE 7. Full-scale test using the sub-assemblage frame test method Source: own work.



FIGURE 8. Deformation in the SAR-200 specimen Source: own work.

The failure process of bending the web beam under the applied load occurred (Fig. 9). Lateral-torsional buckling of the beam caused crushing on the top flange and web. The midspan failure was due to twisting induced by this buckling.

The failure mode occurred because the top flange was the most vulnerable component (Fig. 10). The test ended due to lateral-torsional buckling, which led to a reduction in the applied load. The flange deformation occurred with compression observed at both the top and bottom due to the load applied to the beam (Fig. 11).



FIGURE 9. Failure on the beam's top flange

Source: Own work



FIGURE 10. Lateral-torsional buckling of the beam

Source: own work.



FIGURE 11. Crushing failure on the beam's top flange

The bearing failure modes occurred on the joint for SAR specimens (Fig. 12). The failure occurred due to the thinness of the CFS section on both the beam and column.

For SARFC specimens, bearing failure also occurs on the beam and column. The bearing failure is shown in Figure 13. The bearing failure occurred due to the thinness of the CFS section.

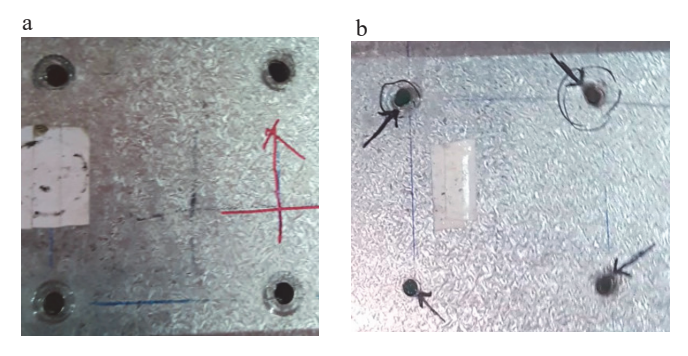


FIGURE 12. Typical failure modes of SAR specimens on (a) column and (b) beam Source: own work.

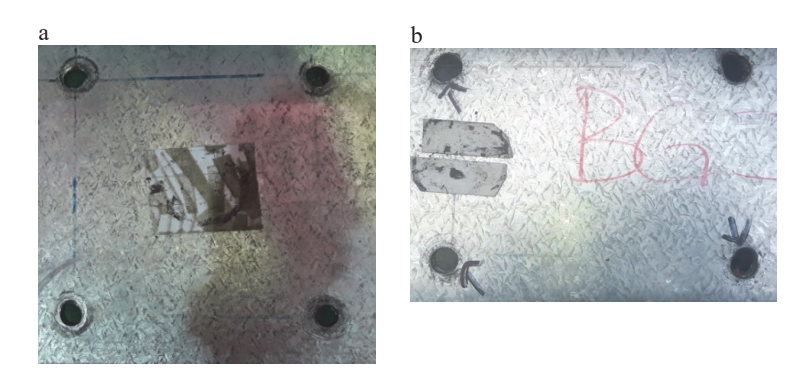


FIGURE 13. Typical bearing failure modes of SARFC specimens on (a) column and (b) beam Source: own work.

Failure of the flange cleat was observed on SARFC specimens (Fig. 14). The bending of the column flange (Fig. 14) is due to the tensile force occurring on the bolts between the flange cleat and the column. In the compression zone, the buckling of the flange-cleat occurs. The failure indicated that the compression zone sustained greater damage to the flange cleat.



FIGURE 14. Typical failure modes of SARFC specimens on the joint Source: own work.

The bearing failure mechanisms appeared on the joint for SAH specimens (Fig. 15). The thinness of the CFS section in both the beam and column led to insufficient load-bearing capacity, which ultimately resulted in the observed failures.

The experiment data were recorded in the data logger. The load was analyzed concerning deflection to establish the relationship between load and beam resistance. Graphs were generated to visualize this correlation between load and deflection.

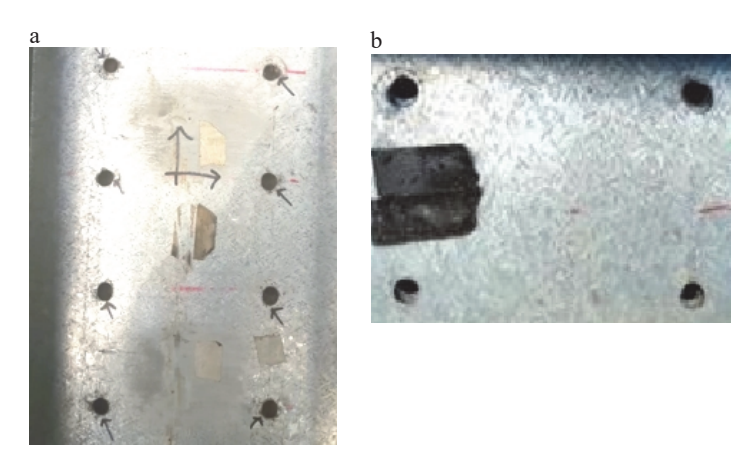


FIGURE 15. Typical failure modes of HG specimens on the joint Source: own work.

The beam's deflection was measured with LVDTs positioned to determine the maximum deflection. Ensuring the load is at the deflection limit under the service limit state is crucial. Enhanced connection rigidity reduces beam bending. The load-deflection relationship was analyzed at the midpoint of the specimen, specifically at the position of LVDT-1. The maximum allowable deflection at the beam's midpoint is specified by Eurocode 3 (category: beams carrying plaster or other brittle finishing):

$$\delta_{360} = \frac{L}{360} = \frac{4,000 + 300}{360} = 11.94 \text{ mm} \tag{1}$$

$$\delta_{200} = \frac{L}{200} = \frac{4,000 + 300}{200} = 21.5 \text{ mm}$$
 (2)

where: L is the distance between the midpoints of two columns. This limitation determines the maximum load that the beam can support with the designed connection.

The load for allowed deflection is obtained from the test using the acceptable deflection formula. P_{200} denotes the load corresponding to a deflection of L/200, whereas P_{360} indicates the load at a deflection of L/360. The graphs illustrate the correlation between load and deflection for the SAR-200 and SAR-250 models (Figs. 16 and 17). The SAR-200 maintains a maximum load of 68.82 kN and demonstrates a maximum deflection of 26.19 mm. The maximum allowable load for P_{200} is 59.04 kN, but for P_{360} it is 34.21 kN.

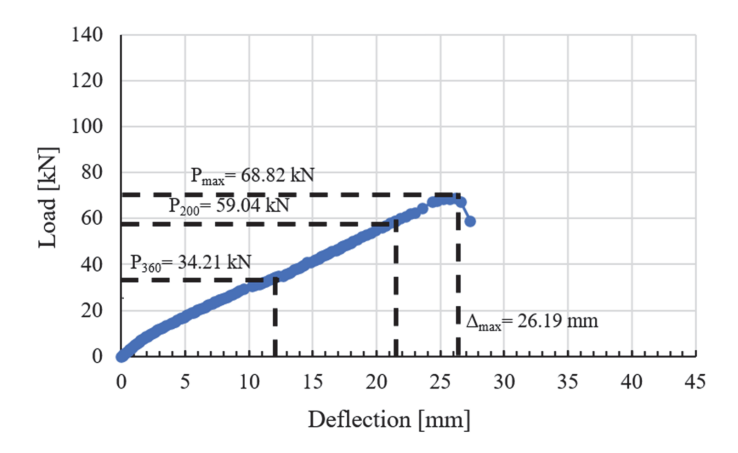


FIGURE 16. Load-deflection relation curve for SAR-200

Figure 16 illustrates the load–deflection relationship for SAR-250. The maximum load, denoted as $P_{\rm max}$, is 83.58 kN, while the maximum deflection is recorded as 27.06 mm. The maximum allowable load for P_{200} is 70.79 kN, whereas for P_{360} it is 45.35 kN.

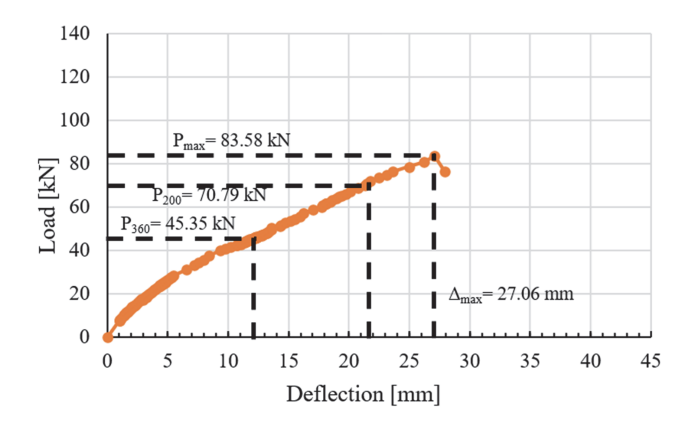


FIGURE 17. Load-deflection relation curve for SAR-250

Source: own work.

The SARFC-200 accommodates a maximum load of 103.63 kN with a deflection of 39.07 mm (Fig. 18). The maximum load for P_{200} is 64.30 kN, while P_{360} has a maximum load of 38.76 kN. The load-deflection graph of SARFC-250 indicates a $P_{\rm max}$ of 122.60 kN and a maximum deflection of 28.76 mm (Fig. 19). The allowable load limit for P_{200} is 98.03 kN, whereas for P_{360} it is 61.26 kN.

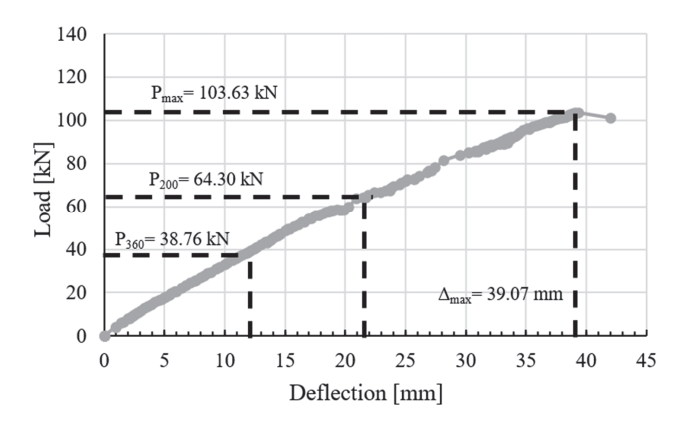


FIGURE 18. Load-deflection relation curve for SARFC-200

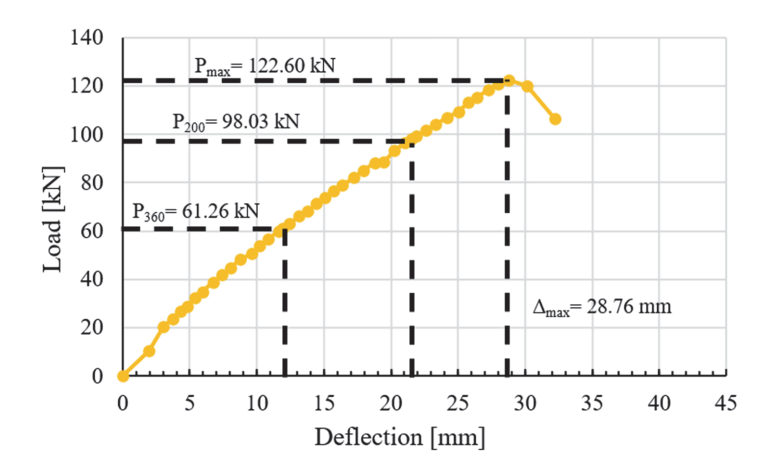


FIGURE 19. Load-deflection relation curve for SARFC-250

The SAH-200 accommodates a maximum load of 108.86 kN with a deflection of 36.38 mm (Fig. 20). The maximum load for P_{200} is 74.34 kN, while P_{360} has a restriction of 45.40 kN. The load-deflection graph of SAH-250 exhibits a maximum load ($P_{\rm max}$) of 124.73 kN and a maximum deflection of 25.78 mm (Fig. 21). The permissible load limit for P_{200} is 112.51 kN, whereas for P_{360} it is 68.64 kN.

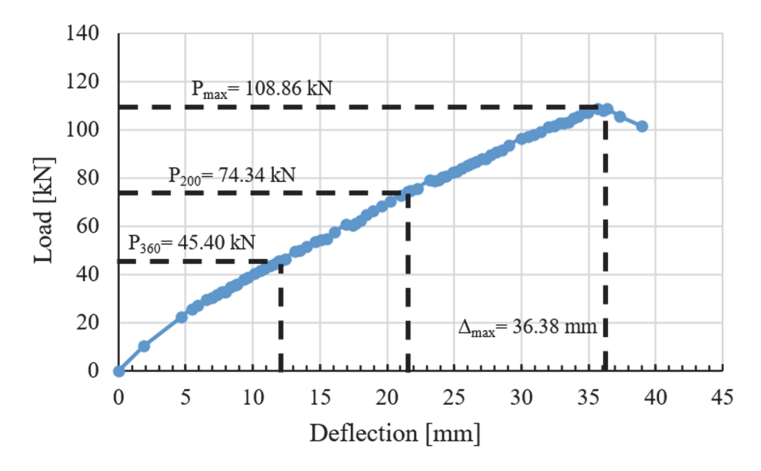


FIGURE 20. Load-deflection relation curve for SAH-200

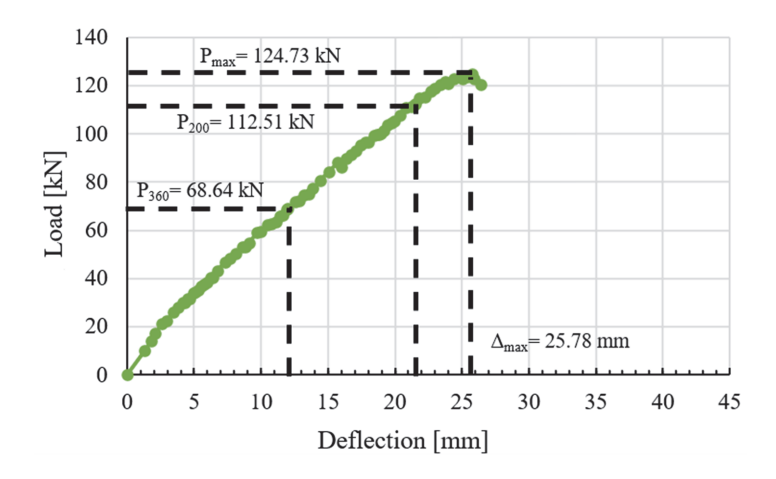


FIGURE 21. Load-deflection relation curve for SAH-250

The SAH-250 specimen has the highest maximum load ($P_{\rm max}$), while the SAR-200 specimen reveals the lowest (Table 4). SAR and SARFC connections possess a decreased load capacity relative to SAH, related to the gusset plate shape, which inhibits excessive beam deflection and results in more resilient connections. SAH-200 has a maximum load that is 55.03% more than that of SAR-200 and 6.94% higher than SARFC-200. SAH-250 has a maximum load that is 42.22% more than that of SAR-250 and 5.00% higher than SARFC-250. The SAH-250 has a maximum load that exceeds that of the SAH-200 by 14.58%. It shows that the height of the beam influences the beam deflection and the load capacity. The taller the beam, the more it increased the load capacity and decreased the beam deflection.

TABLE 4. Summary of load and deflection curves

Specimen	$P_{ m max}$ [kN]	$\delta_{ m max}$ [mm]	P ₃₆₀ [kN]	P ₂₀₀ [kN]
SAR-200	70.22	26.72	34.29	59.43
SAR-250	87.70	28.39	46.25	71.50
SARFC-200	101.8	38.38	38.67	64.34
SARFC-250	118.8	27.87	60.73	97.14
SAH-200	108.86	36.38	45.40	74.34
SAH-250	124.73	25.78	68.64	112.51

The utilization of flange cleats on SARFC also increases the load capacity significantly compared to SAR specimens. The SARFC-200 specimen has a load capacity 44.97% higher than the SAR-200, while the SARFC-250 has a load capacity 35.46% higher than the SAR-250. The influence of beam height shows that SARFC-250 has a load capacity 16.70% higher than SARFC-200.

Thus, the shape of the gusset plate, the height of the beam, and the utilization of flange cleats have a significant role in determining the load capacity and deflection of connections. Therefore, choosing the appropriate gusset plate shape, beam height, and the addition of a flange cleat is crucial for ensuring resilient connections in structural design.

Conclusions

A study was conducted on the SAFT of a cold-formed steel beam-column connection. The key conclusions are:

- SAH-250 has enhanced load capacity relative to other specimens, owing to the different type of gusset plate and an increased beam depth. SAH-250 has a maximum load that is 42.22% higher than SAR-250, while SAH-250 has a maximum load that exceeds SAH-200 by 14.58%.
- The utilization of flange cleats on rectangular gusset plates minimizes the difference of load capacity to haunched gusset plates by 6.94% for the C200 beam and 5% for the C250 beam. It shows that the utilization of flange cleats on SARFC also increases the load capacity significantly compared to SAR specimens by 44.97% for the C200 beam and 35.46% for the C250 beam.
- Failures observed in the specimens are consistent, including buckling of the beam's flange and web, as well as lateral torsional buckling.
- All of the specimens experienced bearing failure in the bolt hole in the beam and column. Additionally, a flange cleat failure occurred on the SARFC specimen.

Recommendations for future research include changing the beam profile to a sigma-type profile, or adding a stiffener on the web or flange to increase the stiffness of the CFS beam. Increasing the stiffness of the CFS beam may enhance its load-bearing capacity and overall structural performance. Future studies could also explore the effects of different materials or composite reinforcements to further improve the beam's resilience under various loading conditions. Additionally, investigating the impact of optimized geometric configurations and innovative

connection methods could yield significant insights into maximizing the efficiency of CFS beams. By combining these approaches, researchers may develop advanced solutions that not only improve structural integrity but also reduce material usage and construction costs.

References

- Aminuddin, K. M., Saggaff, A., Tahir, M. M., Ngian, S. P., Sulaiman, A., Firdaus, M., & Salih, M. N. (2020). Behaviour of rectangular gusset plate with angle cleat connections for cold-formed steel section. *IOP Conference Series: Materials Science and Engineering*, 849(1), 012068. https://doi.org/10.1088/1757-899X/849/1/012068
- Bondok, D., Salim, H., & Urgessa, G. (2021). Quasi-static responses and associated failure mechanisms of cold-formed steel roof trusses. *Engineering Structures*, 231, 111741. https://doi.org/10.1016/j.engstruct.2020.111741
- Chen, X., Blum, H., Roy, K., Pouladi, P., Uzzaman, A., & Lim, J. B. (2021). Cold-formed steel portal frame moment-resisting joints: Behaviour, capacity and design. *Journal of Constructional Steel Research*, 183, 106718. https://doi.org/10.1016/j.jcsr.2021.106718
- Dar, M. A., Subramanian, N., Baniya, M. G., Anbarasu, M., Carvalho, H., & Dar, A. R. (2021). Development of an efficient steel truss system using CFS sections: a comparative study with a hot-rolled steel truss. *International Journal of Structural Integrity*, 12(6), 894–903. https://doi.org/10.1108/IJSI-06-2020-0060
- Dubina, D., Ungureanu, V., & Landolfo, R. (2012). Design of cold-formed steel structures: Eurocode 3: design of steel structures. Part 1–3: design of cold-formed steel structures. Wiley Online Library. https://doi.org/10.1002/9783433602256
- El-Hadary, M. R., El-Aghoury, I. M., & Ibrahim, S. A-B. (2022). Behavior of different bolted connection configurations in frames composed of cold-formed sections. *Ain Shams Engineering Journal*, *13*(1), 101500. https://doi.org/10.1016/j.asej.2021.05.014
- European Committee for Standardization [CEN]. (2005). *Eurocode 3: Design of steel structures*. *Part 1–1: General rules and rules for buildings* (EN 1993-1-1).
- European Committee for Standardization [CEN]. (2006). Eurocode 3: Design of steel structures. Part 1–3: General rules Supplementary rules for cold-formed members and sheeting (EN1993-1-3).
- Firdaus, M., Saggaff, A., Tahir, M. M., Aghlara, R., Sulaiman, A., Aminuddin, K., Ngian, S. P., Salih, M. N. A. (2020a). Influence of seat angles on the behaviour of cold-formed steel concrete composite joints. *Journal of Constructional Steel Research*, 173, 106246. https://doi.org/10.1016/j.jcsr.2020.106246
- Firdaus, M., Saggaff, A., Tahir, M. M., & Poi, S. (2020b). Experimental study of combined gusset plate with flange web cleat connection in sustainable, isolated and sub-assemblage of cold-formed steel. *Journal of Green Engineering*, 10, 13132–13149.

- Fitrah, R. A., & Nofriyandi, R. (2020). The performance between two long-span roof trusses of cold formed steel with back to back channel section. *IOP Conference Series: Materials Science and Engineering*, 846(1), 012060. https://doi.org/10.1088/1757-899X/846/1/012060
- Harini, B., Lingeshwaran, N., Perumal, K., & Aravinthan, K. (2020). Sustainable design of cold formed steel. *Materials Today: Proceedings*, 33, 881–885. https://doi.org/10.1016/j. matpr.2020.06.406
- Johnston, R. P., McGrath, T., Nanukuttan, S., Lim, J. B., Soutsos, M., Chiang, M. C., Masood, R., & Rahman, M. A. (2018). Sustainability of cold-formed steel portal frames in developing countries in the context of life cycle assessment and life cycle costs. *Structures*, 13, 79–87. https://doi.org/10.1016/j.istruc.2017.11.003
- Pouladi, P., Ronaldson, J., Clifton, G. C., Ingham, J. M., Wrzesien, A. M., & Lim, J. B. (2019). Finite-element assisted design of eaves joint of cold-formed steel portal frames having single channel-sections. *Structures*, 20, 452–464. https://doi.org/10.1016/j.istruc.2019.05.009
- Seok, S., Lee, J., Choi, C. S., & Hwang, S. H. (2022). A practical design of cold-formed steel bolted moment connection: numerical investigation with an improved bolt slip-bearing model. *Journal of Building Engineering*, 62, 105345. https://doi.org/10.1016/j.jobe.2022.105345
- Song, L., Yan, W., Zhang, X., Yu, C., & Xie, Z. (2020). Feasibility research on the application of self-piercing riveted connection in cold-formed steel structures. *Journal of Constructional Steel Research*, *168*, 105957. https://doi.org/10.1016/j.jcsr.2020.105957
- Wang, F., Han, Y., & Yang, J. (2021). Nonlinear FE analysis on stiffness and resistance of bolted cold-formed steel built-up joints. *Structures*, *33*, 2520–2533. https://doi.org/10.1016/j.istruc.2021.04.098
- Ye, J., Mojtabaei, S. M., & Hajirasouliha, I. (2019). Seismic performance of cold-formed steel bolted moment connections with bolting friction-slip mechanism. *Journal of Constructional Steel Research*, *156*, 122–136. https://doi.org/10.1016/j.jcsr.2019.01.013
- Yu, W. W., LaBoube, R. A., & Chen, H. (2019). Cold-formed steel design. Wiley.

Summary

Investigation of failure modes and load-deflection of cold-formed steel connections using sub-assemblage frame tests. Cold-formed steel (CFS) is a type of steel manufactured at ambient temperature using bending and rolling methods, enabling enhanced precision in shape and sizing. Its adaptability, resilience, and environmental sustainability render it very beneficial for building. Furthermore, its manufacturing method is more energy-efficient than conventional steel production and decreases emissions. Nonetheless, CFS has several limitations, including vulnerability to buckling owing to its slender profile. This research especially examines beam-column constructions with cold-formed steel connections. The paper discusses an experiment utilizing the sub-assemblage frame test method to improve the connection's resistance by emphasizing haunched gusset plates, rectangular gusset plates, and a combination of rectangular gusset plates with the top-seat

angle. The results demonstrated that the lateral-torsional buckling occurred on the beam. The connection's bolt hole exhibited a bearing failure, and the flange cleat also experienced buckling. Graphs were employed to examine the load and deflection data, with maximum load and deflection values documented for each specimen. The result shows that the type of gusset plate, the height of the beam, and the utilization of flange cleats have an impact on the performance of the connection.